13th World Conference on Earthquake Engineering
Vancouver, B.C., Canada
August 1-6, 2004
Paper No.590

LIQUEFACTION FLOW ANALYSIS OF URBAN RIVER DIKE BY DISTINCT ELEMENT METHOD

Hiroshi MORI[1], Yoshimi OGAWA[2] and Guoqiang CAO[3]

SUMMARY

We have developed a liquefaction flow analysis method by Distinct Element Method (DEM) with granular assemblies, in which the excess pore water pressure is taken into account to estimate the large permanent displacement by liquefaction, and applied that method to urban river dikes (Yodo-gawa river dike in Osaka and Naka-gawa river dike in Tokyo). In this analysis, DEM is composed of a constitutive model which based on the mechanical model of elasto-plastic body introducing shear springs and sliders representing stress-strain relationships following Masing's rule. The buildup of excess pore water pressure among these shear springs is evaluated by the dissipative energy and stored elastic energy of a soil.

The vertical displacement of embankment crest in Yodo-gawa river dike damaged by the 1995 Hyogoken-Numbu earthquake obtained by DEM exhibits good agreement with the actual measured maximum vertical permanent displacement. And, the vertical displacement of embankment crest in damaged model is larger than that of non-damaged model with a major bed. Despite different disc radii (R=30,15,7.5cm), the results of analysis yield no significant difference. The deformation of Naka-gawa river dike utilized the improved ground method (Deep Mixing Method) with steel pipe pile for the seismic resistance of earth-structure is smaller than the deformation at the existing Naka-gawa river dike which used thin sheet piles only in front of the revetment. The zone occupied liquefied areas of the former expressed by excess pore water pressure ratio is much smaller than that of the latter. The effect of improved ground planning to construct at land side in the near future was observed by this analysis method. This method can indicate the effectively of improved ground method or steel pipe pile to prevent from liquefaction flow, and provide satisfactorily enough estimation to correlate results of real disaster.

INTRODUCTION

Tokyo has a number of river dikes below-sea level areas called "Tokyo lowlands" shown in **Figure 1**. Because the deposit in Tokyo lowlands generally exhibits a thick soft soil layer, it is very important to study the behavior of ground foundation for the mitigation of earthquake disaster (Mori et al. [1]). In view of the growing public demand for the cost-effectiveness improvement and cost reduction, the development of a

[1] Researcher, Tokyo Metropolitan Government, Tokyo, JAPAN. Email: mori@doken.metro.tokyo.jp
[2] Researcher, Tokyo Metropolitan Government, Tokyo, JAPAN. Email: ogawa@doken.metro.tokyo.jp
[3] Analysis Engineer, CRC Solutions, Inc., Tokyo, JAPAN. Email: soh@crc.co.jp

reasonable earthquake resistant design method is now strongly required. In fact, all below-sea areas dikes consist of a thin shaped revetment with a retaining structure designed to protect against high flood. Part of the river dike has already been constructed as the huge river dike (super levee) including a land side of river dike. In reality, however, it is impossible to take full advantage of a land side in Tokyo because a number of people live near river side. Also, it is well known that, the major cause of Yodo-gawa river dike damaged by the 1995 Hyogoken-Numbu earthquake in Osaka, was the liquefaction of the ground where the loose sand layer exists. For these reasons, Tokyo Metropolitan Government is implementing a high priority earth-quake-proof project for river dikes presently.

Figure 2 shows the severely damaged cross section of Torishima area (Damaged model) located near the Yodo-gawa river mouth within about 40km from the epicenter (Abe et al. [2]). The concrete parapet wall at the top of embankment slipped into the riverbed and the maximum vertical permanent displacement was about 3.0m. On the other hand, no major damage in Takami area (Non-damaged model) with major bed (flood plane) located in the upper riverside from Torishima area was not observed (Matsuo et al. [3]). Also, **Figure 3(a)** shows the existing Naka-gawa river dike with thin sheet piles only in front on the revetment before the seismic resistance construction. **Figure 3(b)** shows Naka-gawa river dike utilized the improved ground method (Deep Mixing Method; a kind of deep in-situ admixture stabilization of soft ground to use the cement slurry) with steel pipe pile for the seismic resistance.

Recently, the rapid increase of computer abilities has drastically extended availability of DEM. In the field of geotechnical earthquake engineering, liquefaction is one of the most important, complex and necessary topics (Cundall and Strack [4]; Ng and Dobry [5]; Matsushima and Kanagai [6]; Ogawa et al [7]; Mori et al. [8]). In this study, the liquefaction analysis method with which DEM is used to calculate the excess pore water pressure, is utilized to estimate the large permanent displacement caused by liquefaction. This application is applied to Yodo-gawa river dike damaged by the 1995 Hyogoken-Numbu earthquake in Osaka and Naka-gawa river dike with a thin shaped revetment in Tokyo.

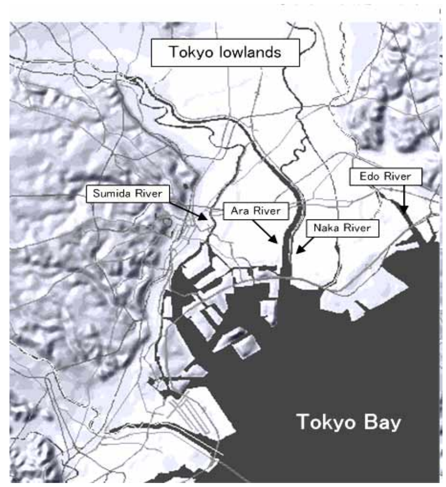

Figure 1 Tokyo lowlands

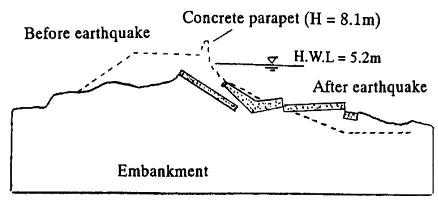

Figure 2 Damaged cross section of Torishima area

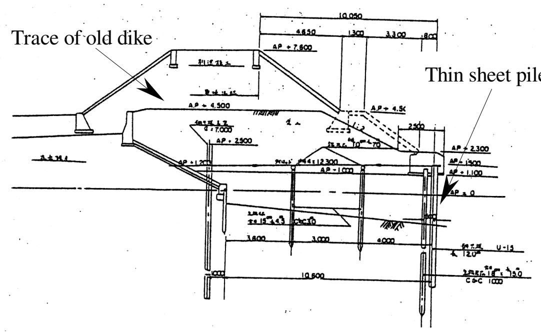

Figure 3(a) Existing Naka-gawa river dike

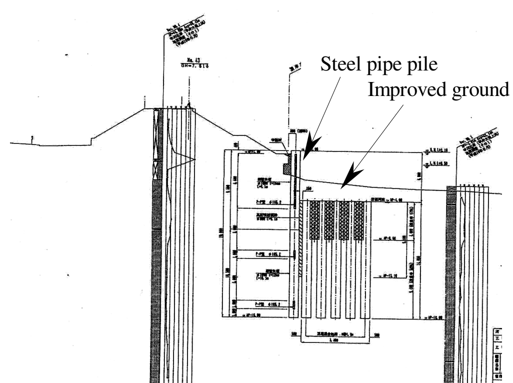

Figure 3(b) Naka-gawa river dike after constructing for the seismic resistance

DISTINCT ELEMENT METHOD BASED ON EFFECTIVE STRESS

In this analysis, a calculating program of liquefaction flow based on the effective stress method is incorporated into the DEM program (Code name: *PFC*^{2D}). In this program, the interaction of the circular discs (Balls) is treated as a dynamic process with states of equilibrium calculated by the internal force balance. The calculations performed in this program utilize an explicit finite-difference method alternating between the application of Newton's second law to the circular discs and a force-displacement law at the contacts. The initial effective normal force obtained by the normal spring at the contact of circular discs is calculated from the static self-weight analysis in which gravity force and buoyancy are applied to each disc (see **Figure 4**). The shear spring of DEM is composed of a constitutive model (Iwan parallel model) which based on the mechanical model of elasto-plastic body proposed by Iwan [9]. This model is composed of simple linear springs and Coulomb sliders of friction elements representing stress-strain relationships following Masing's rule as shown in **Figure 5**. The Frictional force based on shear work of the sliding element ($\Delta\tau$) is defined as the following equation (Ogawa et al. [10]):

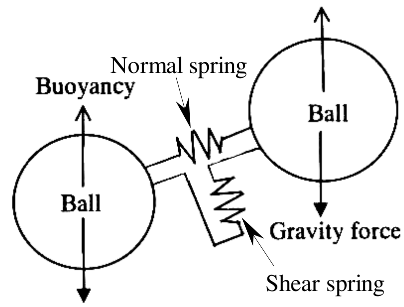

Figure 4 Circular discs (Balls)

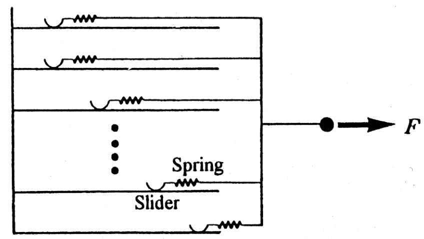

Figure 5 Iwan parallel model

$$\Delta\tau = \Delta G \cdot \gamma \qquad (1)$$

where ΔG is the shear rigidity decrement and γ is the strain amplitude expressed from skeleton curve. The accumulative excess pore water pressure caused by shear force plus the effective normal force is equal to the initial effective normal force. Ogawa et al. [11] have proposed the calculating method to determine the dissipative energy obtained by dislocations of sliders as a continuos function, and the stored elastic energy is calculated as the difference between the shear work and dissipative energy. Thus, the buildup of excess pore water pressure of each spring of DEM is evaluated by the dissipative energy and stored elastic energy of a soil, and development of excess pore water pressure caused by shear force is simulated. The normal force (F^n) at the contact of circular discs is expressed as follows:

$$F^n = F'^n_b + F^n_s + F^n_c \qquad (2) \qquad\qquad F'^n_{b,0} = F'^n_b + F^n_s \qquad (3)$$

where F'^n_b is the effective normal force, F^n_s is the excess pore water pressure at shear work and F^n_c is the excess pore water pressure at compressive and expansive work. The initial effective normal force ($F'^n_{b,0}$) is defined to coincide with the value obtained by the static self-weight analysis in which gravity force and buoyancy are applied to each disc. Also, assuming that the alteration of relative displacement in the normal direction obtained by the static self-weight analysis is converted into F^n_c entirely, F^n_c is given as the following equation:

$$F^n_c = F^n - F'^n_{b,0} = K_n \cdot u^n - F'^n_{b,0} \qquad (4)$$

where K_n is the stiffness of normal spring and decided to base on bulk modulus of a soil, u^n is the relative displacement in the normal direction. The shear force (F'^s) at the contact of circular discs is defined as;

$$F'^s = \frac{F'^n_{b,0}}{\sigma_{ini}} \cdot \frac{F'^n_b}{F'^n_{b,0}} \cdot T = \frac{F'^n_b}{\sigma_{ini}} \cdot T \qquad (5) \qquad\qquad F'^s_0 = \frac{F'^n_{b,0}}{\sigma_{ini}} \cdot T \qquad (6)$$

where σ_{ini} is the initial effective confining stress defined by establishing Iwan model and T is the shear stress calculated from Iwan parallel model at the given strain that represents histeresis loops according to Masing's rule. Especially, the shear strain increment ($\Delta\gamma$) is given as the following equation:

$$\Delta\gamma = \frac{u^s}{2R} \qquad (7)$$

where u^s is the relative displacement in the shear direction and R is the radius of circular disc. Then, F'^s_0 is the initial shear force obtained by the static self-weight analysis. According as a decrease or increase in excess pore water pressure, F^n_s is estimated on the assumption that the energy calculated from compression is proportional to the square root of the dissipative energy (E'_l) and the energy done from expansion is proportional to the stored elastic energy (E'_p), and is given as the following equation:

$$F^n_s = K\left(\varepsilon_n + \varepsilon_p\right) \qquad (8)$$

where K is the bulk modulus, ε_n is the compressive volumetric strain and ε_p is the expansive volumetric strain. Ogawa [12] has proposed the constitutive equations to consider dilatancy from these energies. ε_n with negative dilatancy and ε_p with positive dilatancy are evaluated from the dissipative energy and stored elastic energy, respectively:

$$\frac{1}{2} \cdot \frac{\varepsilon_n^2}{m_v} = E'_l \cdot \alpha \qquad (9) \qquad\qquad F'^n_{b,0} \cdot \varepsilon_p = -E'_p \cdot \beta \qquad (10)$$

where m_v is the coefficient of volume compressibility, α and β are the proportionality constant based on negative and positive dilatancy. It is supposed that α is less than 1.0 and β is expected to be 1.0.

As mentioned above, in case of sandy soil, we take the relationship of the equation (5) into consideration. On the other hand, as the proportional law which the shear force varies in obedience to the effective normal stress cannot be applied to clay soil, we employ the shear force based on the following equation.

$$F'^s = S \cdot T \qquad (11)$$

where *S* is the area of contact face between discs in clay soil. *S* has to be decided to change the area to occupy the distinct elements defining the shear force based on the shear spring according as the radius of disc is transformed.

CYCLIC SIMPLE SHEAR TEST

The parameters of DEM in this analysis are determined as shown in **Figure 6**. According to consider the primary wave velocity, the stiffness K_n of normal spring at the contact for calculation of contact force between discs in the direction of disc center, is determined to base on the simulation results of the simple shear test and cyclic simple shear test (Meguro and Hakuno [13]; Igarashi and Meguro [14]).

Figure 7 shows the distinct elements of the (cyclic) simple shear test in conditions of the different disc radii (R=30, 15, 7.5cm) to estimate the influences of radii of disc. **Table 1** shows the experimental parameters on which to perform this simulation of the simple shear test or cyclic simple shear test (Abe and Kusano [15]). **Table 2** shows the parameters for analysis determined by the flowchart shown in **Figure 6**. In case of R=30cm with τ_d / σ_{ini} (initial shear stress ratio)=0.14, **Figure 8** shows both the relationship between $\varepsilon_x + \varepsilon_y$ (volumetric strain) and $(\sigma_x + \sigma_y)/2$ (mean principal stress) and the relationship between γ (shear strain) and τ (shear stress) by analysis in simple shear test. Also, **Figure 9** shows the relationships between K (bulk modulus), G (shear modulus), τ (shear stress) and disc radius in cases of R=30, 15, 7.5cm. K and G observed from **Figure 8** are fit in a linear shape and τ is assumed to treat as an average value. Despite different disc radii, the results of analysis for simple shear test are approximately identical with experimental results obtained by real specimen test. **Figure 10(a)** shows relationships between the excess pore water pressure ratio (U / σ_{ini}) and the number of cycles (N) for the case of R=30cm under conditions of the different initial shear stress ratios (τ_d / σ_{ini}) in cyclic simple shear test. For the sake of convenience, it also indicates the development of initial effective confining stress ratio (σ / σ_{ini}) in the same figure. Each excess pore water pressure tends to coincide with the initial effective confining stress. The excess pore water pressure ratio of τ_d / σ_{ini} =0.20 achieves the complete liquefaction faster than that of τ_d / σ_{ini} =0.14. In cases of R=15 and 30cm with τ_d / σ_{ini} =0.14, the relationships between the excess pore water pressure ratio and the number of cycles are shown in **Figure 10(b)**. Although the development of excess pore water

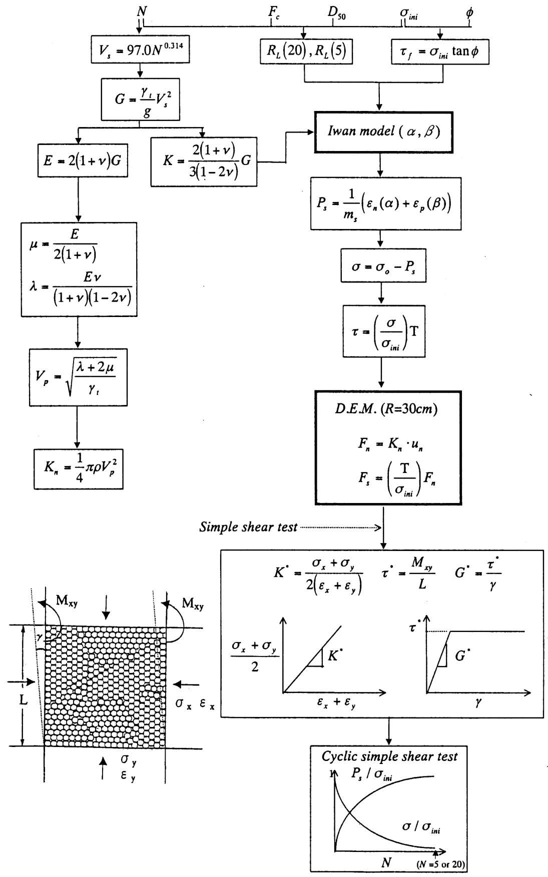

Figure 6 Flowchart for determination of parameters

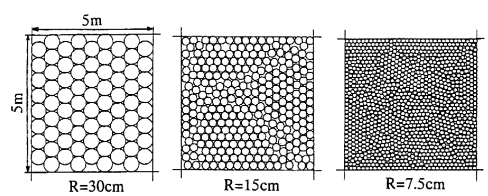

Figure 7 Distinct elements for (cyclic) simple shear test

Table 1 Experimental parameters

σ_{ini}	98.1 kPa
G	73,600 kPa
K	98,133 kPa
τ_f	59.0 kPa
τ_d	29.4 kPa
N	5
τ_d	20.6 kPa
N	20

Table 2 Parameters for analysis

$\sigma_{ini}^{(i)}$	98.0 kPa
$G^{(i)}$	73,600 kPa
K_n	200 MN/m
$\tau^{(i)}_{max}$	59.0 kPa
M^*	50
α	0.14
β	1.02

M^*: Number of element by Iwan model

pressure ratio in the case of *R*=30cm expresses the smoothest performance, it is not recognized the drastic difference between developments of excess pore water pressure ratio in cases of *R*=30, 15, 7.5cm clearly. Moreover, **Figure 11** shows the distribution of excess pore water pressure ratio (0.25, 0.5, 0.75, 1.0) obtained by the cyclic simple shear test in 2.0Hz frequency in cases of *R*=30, 15, 7.5cm, respectively. According as the disc radii are small, it can observe the distribution of excess pore water pressure ratio for cyclic simple shear test clearly. Particularly, in the case of *R*=7.5cm, the distribution of

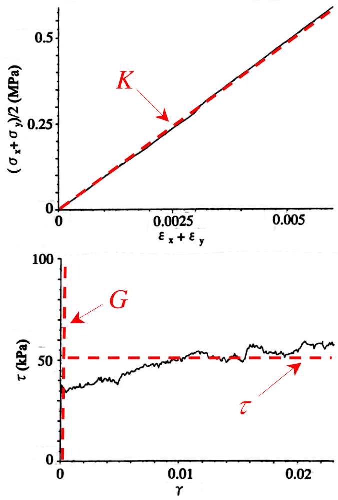

Figure 8 Simple shear test by analysis (*R*=30cm, τ_d / σ_{ini} =0.14)

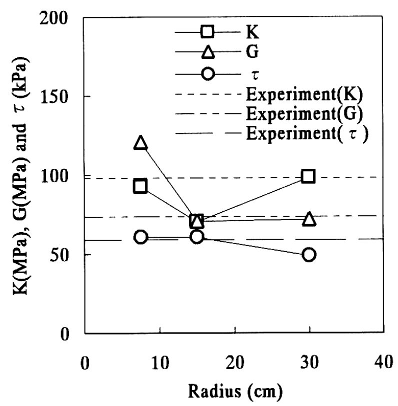

Figure 9 Relationships between *K*, *G*, τ and disc radius

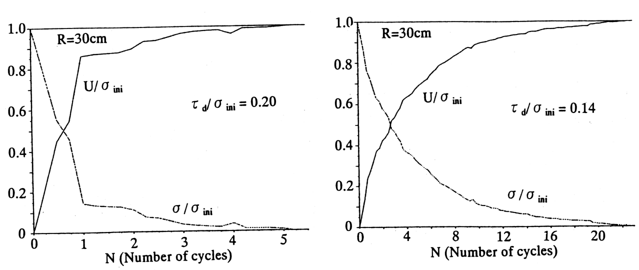

Figure 10(a) U / σ_{ini} and *N* (*R*=30cm)

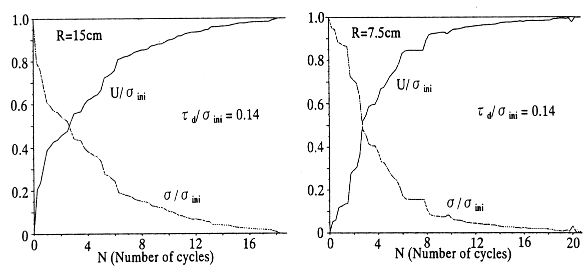

Figure 10(b) U / σ_{ini} and *N* (τ_d / σ_{ini} =0.14)

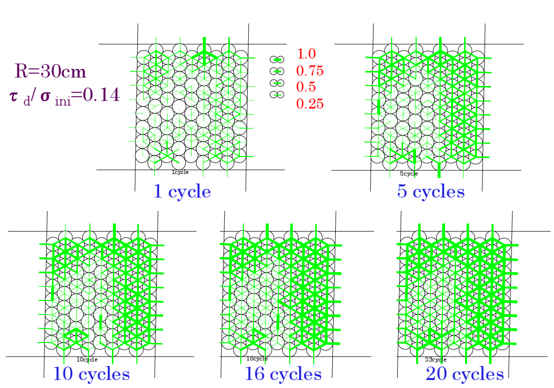

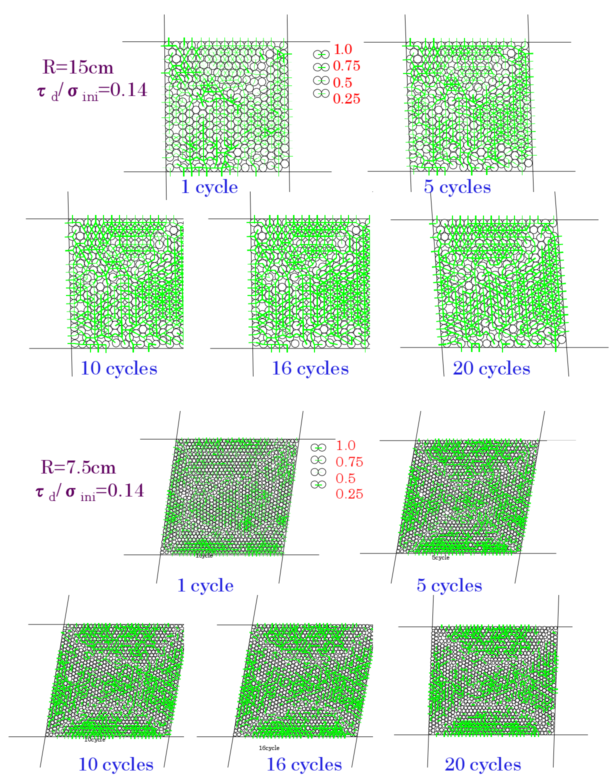

Figure 11 Distributions of excess pore water pressure ratio

excess pore water pressure ratio tends to coincide with the distribution of σ_1 direction inclining to approximately $\pi/4$ from horizontal.

YODO-GAWA RIVER DIKE

Figure 12 shows the ground conditions of a damaged and a non-damaged model at the Yodo-gawa river dike. The deposits at Torishima area consist of sandy layers on the oblique line (No.2, No.3 and No.5), a clay layer (No.4) and a bearing stratum (No.6). The deposits at Takamai area also consist of sandy layers (No.2, No.4 and No.6), a clay layer (No.5) and a bearing stratum (No.7), and the clay layer (No.3) of about 2.0m in thickness is sandwiched between No.2 and No.4. An input wave of 25 second obtained from an accelerometer attached to the bottom of bearing pile located at G.L.-30m near the Takami area shown in **Figure 13**, has the predominant frequency of around 0.5Hz and the maximum acceleration of approximately -138gal. **Figure 14(a)(b)** show the distinct elements (R=30cm and n (porosity) =0.16) of damaged and non-damaged model which are composed of more than ten thousand discs. To build up each compacted model, we employ the radius expansion method to generate the radii to achieve a specified porosity and allow them to move freely until they reach a state of equilibrium within a set of confining walls. **Table 3** shows the parameters of each layer at both sites. Each parameter is determined by considering both results of liquefaction analysis considering the physical property tests at Yodo-gawa river site calcu-

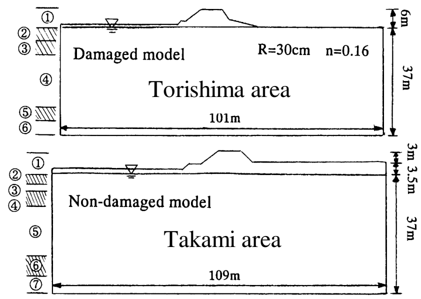

Figure 12 Ground conditions of Yodo-gawa river dike

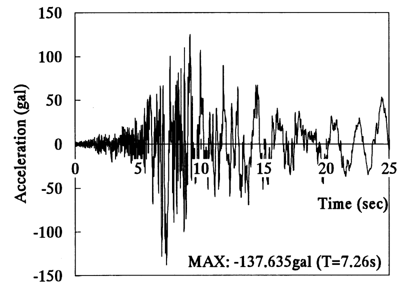

Figure 13 Input wave (Yodo-gawa river dike)

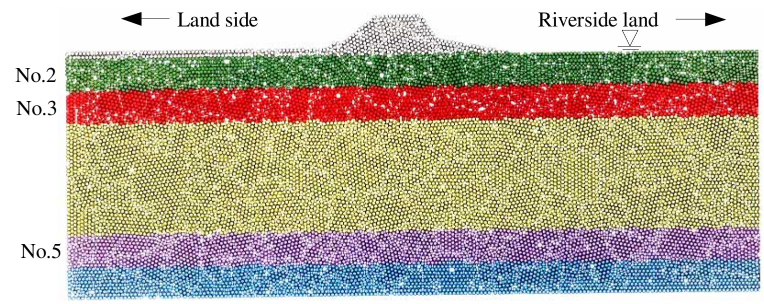

Figure 14(a) Damaged model by analysis

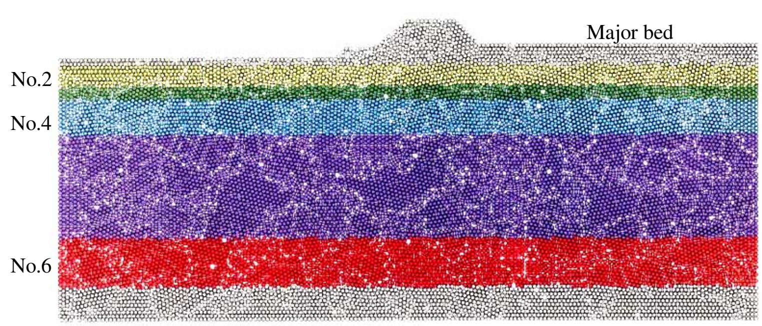

Figure 14(b) Non-damaged model by analysis

Table 3 Parameters by analysis with Yodo-gawa river dike

Damaged model

	Material	γ_t (kN/m^3)	σ_{ini} (kN/m^2)	G (MN/m^2)	$K(\nu=0.45)$ (MN/m^2)	τ_f (kN/m^2)	R_{L20}	α	β	K_n (MN/m)
No.1	Embankment	18.0	55.8	39.06	377.58	39.1	-	-	-	394
No.2	Sand	19.0	134.1	58.83	568.69	87.1	0.191	0.28	0.6	593
No.3	Sand	19.5	180.4	84.40	815.87	146.0	0.251	0.40	0.7	851
No.4	Clay	16.5	259.4	34.75	335.92	202.6	-	-	-	351
No.5	Sand	19.5	338.4	120.91	1168.80	283.9	0.291	0.42	0.8	1220
No.6	Bearing stratum	18.0	382.1	73.62	711.66	298.5	-	-	-	742

Non-damaged model

	Material	γ_t (kN/m^3)	σ_{ini} (kN/m^2)	G (MN/m^2)	$K(\nu=0.45)$ (MN/m^2)	τ_f (kN/m^2)	R_{L20}	α	β	K_n (MN/m)
No.1	Embankment	18.0	58.5	40.95	395.85	41.0	-	-	-	413
No.2	Sand	19.0	130.5	57.25	553.42	84.7	0.253	0.13	0.6	578
No.3	Clay	16.5	150.5	20.17	194.98	117.6	-	-	-	203
No.4	Sand	19.5	180.75	84.59	817.70	146.4	0.244	0.42	0.7	853
No.5	Clay	16.5	253.25	33.93	327.99	197.9	-	-	-	342
No.6	Sand	19.5	335.25	119.80	1158.07	281.3	0.292	0.42	0.8	1208
No.7	Bearing stratum	18.0	388.5	74.85	723.55	303.5	-	-	-	755

lated by Matuo et al. [16] and the flowchart shown in **Figure 6** as mentioned above. **Figure 15(a)(b)** show the deformation of damaged and non-damaged model of Yodo-gawa river dike with the distribution of excess pore water pressure ratio expressed by the degree of green color dots (0.2, 0.4, 0.6, 0.8) at 25 second. It takes about one hundred hours to finish calculating in a personal computer of CPU500MHz/500MB. The vertical displacement of embankment crest in the damaged model is larger than that of the non-damaged model. The former exhibits good agreement with the actual measured maximum vertical permanent displacement (about 3.0m). Furthermore, the vertical displacement of embankment crest in the direction of riverbed with the effect of the major bed does not reveal any damage. It indicates that it is possible to predict the slope movement toward the riverbed by liquefaction flow realistically. The excess pore water pressure ratios obtained from the shallow sandy layers in the damaged model are higher slightly than that of non-damaged model. The occupied liquefied zone area within the shallow sandy layers below the embankment are larger than those below the riverbed.

Figure 16 shows the deformation of damaged model with distribution of excess pore water pressure ratio at 25 second in conditions of the different disc radii (*R*=30, 15, 7.5cm) to check the influence of radii of

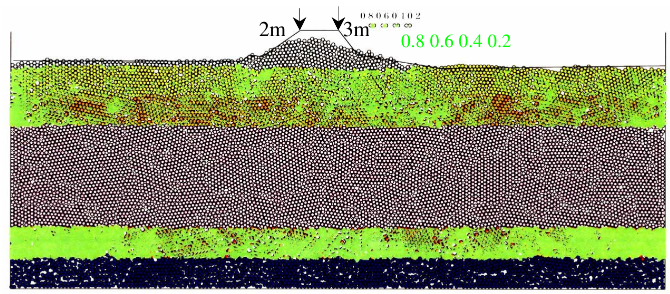

Figure 15(a) Deformation of damaged model with excess pore water pressure ratio

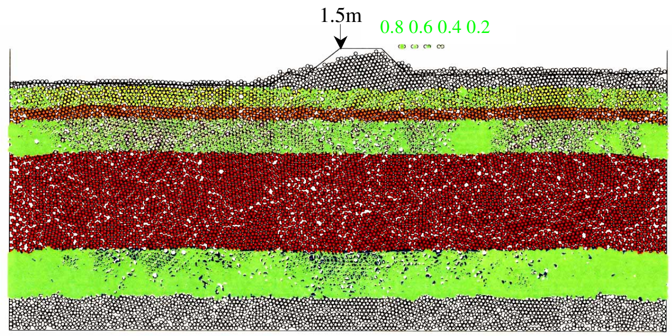

Figure 15(b) Deformation of non-damaged model with excess pore water pressure ratio

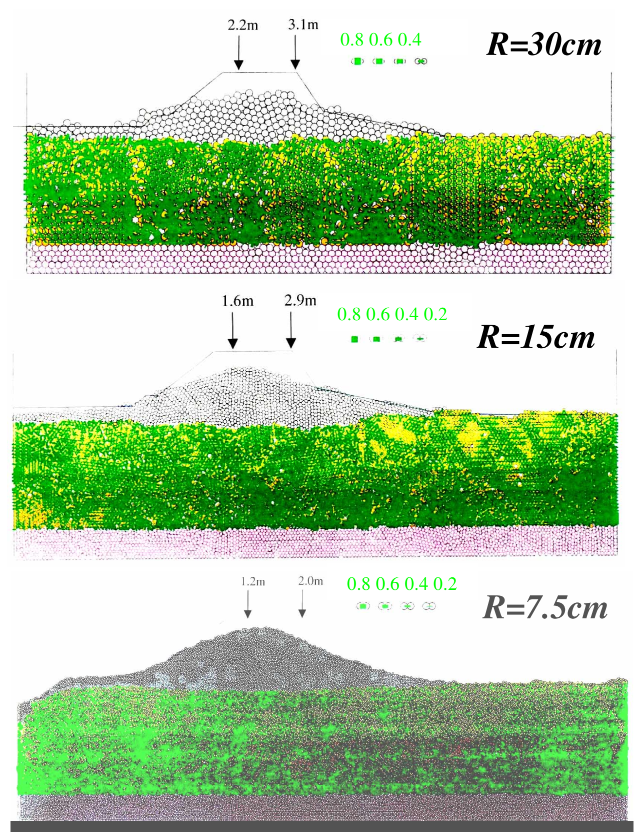

Figure 16 Deformation with excess pore water pressure ratio in conditions of different disc radii

disc. As forecasted to take time to calculate them, it investigates to use the distinct elements (n=0.16) reducing the scale of these models within the limits of values which is possible to compare with the result of **Figure 15(a)**. In this analysis, as the area (S) of contact face shown in equation (11) is assumed to be 1.0 for convenience's sake, the difference of deformation at these embankment crests would appear. According as the disc radii are small, the vertical permanent displacement of embankment crest tends to decrease relatively. As considering the cost performance or calculative effectiveness and so on under the present condition, however, we think that it would be improbable to disturb in performing the analysis using this model of R=30cm.

NAKA-GAWA RIVER DIKE

Now, Naka-gawa river dike is advanced to plan and construct for the seismic resistance. Particularly, it is noteworthy that the Naka-gawa river dike located near the river mouth has a thick sandy layer on a soft clay layer. The method of seismic resistance for the liquefaction adopted by Tokyo Metropolitan Government is generally the improved ground method (Deep Mixing Method) with steel pipe piles. In fact, all most river dike with an embankment has been designed to use the most widely accepted circular slip method (limit equilibrium method) based on design horizontal seismic coefficient (kh=0.18). Generally, the practicing engineering estimates the seismic resistance to employ the relationships between the safety factor (Fs) and the crest settlement of embankment (H: height of embankment) shown in **Table 4**, for example. However, it is not always enough to estimate the effectiveness of seismic resistance against the real disaster. Also, the problem of interaction between the ground foundation and structures (For example; pile structure, retaining structure, tunnel structure, pipe structure, etc) is very important for numerical analyses. For the first time, it tries to compare, the behavior of single pile obtained from Chang's equation [17] that solved a differential equation based on the elastic support beam theory, with the results of analaysis. In the next place, it performs analysis in Naka-gawa river dike with the seismic resistance method.

Table 4 Safety factor and crest settlement

Fs (kh)	Fs (Δu)	Crest settlement
1.0<Fs		0
0.8<Fs≦1.0		H×0.25
Fs≦0.8	0.6<Fs≦0.8	H×0.50
-	Fs≦0.6	H×0.75

Table 5 Parameters of single pile by analysis

Force (F) acted on pile	1.0×10^5 N
Radii of disc (R) of pile	15.0 cm
Modulus of elasticity (E) of pile	2.06×10^5 MN/m²
Moment of inertia (I) of pile	1.49×10^{-4} m⁴/m
Radii of disc (R) of soil	30.0 cm
Modulus of elasticity (E) of soil	1.00×10^2 MN/m²
Density (γ_t) of soil	17.7 kN/m³
Stiffness of normal spring (K_n) of soil	3.60×10^2 MN/m²
Stiffness of shear spring (K_s) of soil	3.60×10^2 MN/m²

Table 5 shows the parameters of a single pile assumed a long free-headed pile in this analysis, and **Figure 17** shows results (Bending moment and deformation) obtained by analysis and Chang's equation in five cases performed a force (F) at the top of pile. The parallel-bond model which can transmit both forces and moments between discs is adopted by the constitutive model of pile. A parallel bond is established by a set of elastic springs with contact normal and shear stiffness distributed a rectangular cross-section lying on the contact plane in center of the contact point. Also, Chang's equation is offered as the following equation:

$$\text{Under-ground: } EI\frac{d^4y}{dx^4} + k_h \cdot B \cdot y = 0 \qquad (12) \qquad \text{Over-ground: } EI\frac{d^4y}{dx^4} = 0 \qquad (13)$$

where E is the elastic modulus, I is the moment of inertia, k_h is the coefficient of horizontal subgrade reaction and B is the diameter of pile.

It is difficult to compare results of Chang's equation with those (Case-1) of analysis considered the parameters shown in **Table 5**. Therefore, we investigate the suitability of Chang's equation in different analytical conditions to other cases for maintaining the objectivity. In Case-2, it is assumed that the stiffness of normal and shear springs of distinct elements put at the neighborhood of surface existing about 2m wide is 30 times. And, in Case-3, it is set up not to destroy distinct elements attached fixedly to the pile. Although the results of Case-2 resemble those of Case-1, the results of Case-3 are closely identical with those of Chang's equation. Also, it is set up not to destroy distinct elements attached fixedly around the pile existing about 1m wide in Case-4 and 2m wide in Case-5. Especially, the bending moment of Case-4 dose not coincide with that of Chang's equation. However, The results of Case-5 are identical with those of Chang's equation as well as Case-3. Thus, we utilize the analytical condition of Case-5 which need not be decided by empirical senses to perform the analysis in Naka-gawa river dike with steel pipe pile.

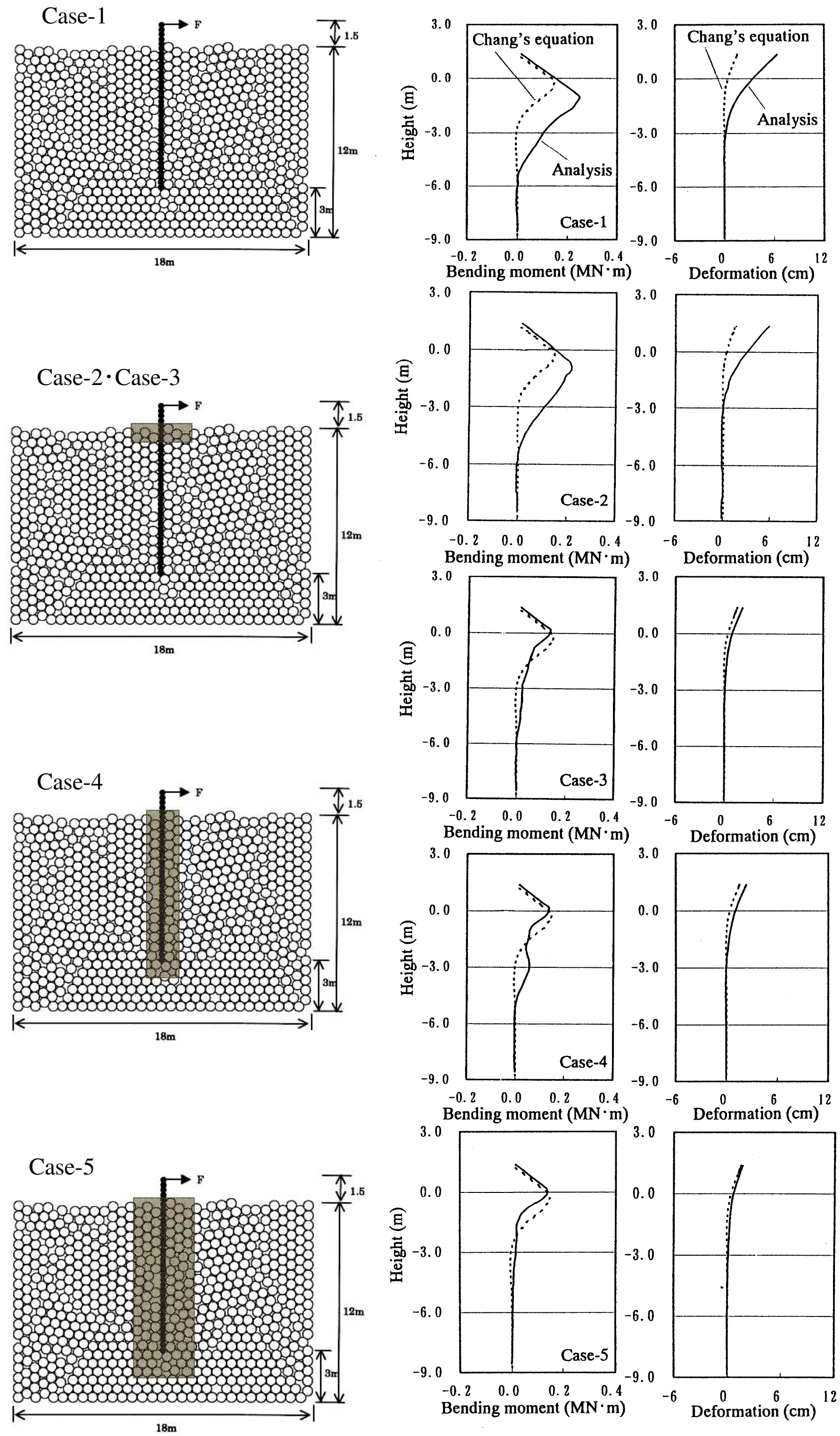

Figure 17 Comparison between analysis and Chang's equation

Figure 18 shows the ground conditions consisting of 8 layers in the improved ground model with steel pipe pile (Height (H) of embankment is about 7m). **Table 6**, **7**, **8** show parameters of steel pipe pile, improved ground and foundation ground of each layer. **Figure 19** shows the distinct elements (R=30cm and n=0.16) by the improved ground model with steel pipe pile composed of more than eight thousand discs. **Figure 20(a)(b)(c)** show the deformation with excess pore water pressure ratio (0.2, 0.4, 0.6, 0.8) at 25 second of the existing model before constructing for the seismic resistance, steel pipe pile model and improved ground model with steel pipe

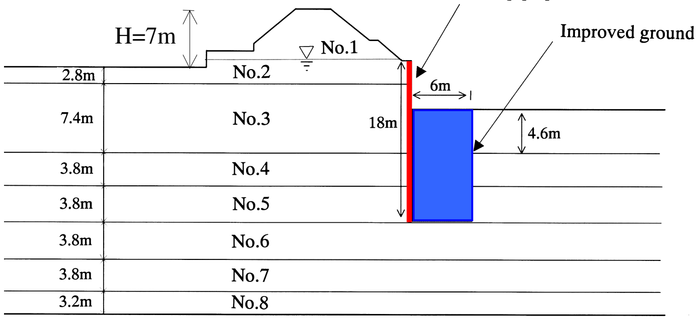

Figure 18 Ground conditions of Naka-gawa river dike

Table 6 Parameters of steel pipe pile

Length (L)	18.0 m
Diameter (D)	100.0 cm
Modulus of elasticity (E)	2.06×10^5 MN/m^2
Moment of inertia (I)	5.69×10^{-3} m^4/m
Flexural stiffness (EI)	1.17×10^3 MN·m^2/m
Sectional area (A)	5.79×10^{-2} m^2/m

Table 7 Parameters of improved ground

No.	Thickness (m)	Area ratio of improvement (%)	Strength of improved ground (kN/m^2)
③	4.6	100	294.3
④	3.8	50	147.2
⑤	3.8	50	147.2

Table 8 Parameters of foundation ground of 8 layers

No	Material	N-value	γ_t (kN/m^3)	ϕ (degree)	c (kN/m^2)	$\sigma'_{v(ini)}$ (kN/m^2)	G (MN/m^2)	K (ν = 0.45) (MN/m^2)	τ_f (kN/m^2)	$R_{L(20)}$	$R_{L(5)}$	α	β	K_n (ν = 0.45, n = 0.16) (MN/m^2)
①	Embankment-A (Sand)	3	16.7	30	-	48.4	31.92	308.59	28.0	-	-	-	-	319.91
②	Embankment-B (Sand)	3	18.6	30	-	109.1	35.68	344.89	63.0	0.19	0.23	0.07	0.21	357.56
③	Sand	9	18.6	35.4	-	154.1	71.12	687.51	109.5	0.24	0.29	0.07	0.19	712.77
④	Clay	3	16.2	-	52.0	198.9	30.98	299.47	52.0	-	-	-	-	310.47
⑤	Clay	2	16.2	-	65.7	223.1	24.01	232.13	65.7	-	-	-	-	240.67
⑥	Clay	2	16.2	-	89.3	247.4	24.01	232.13	89.3	-	-	-	-	240.67
⑦	Clay	4	16.2	-	112.8	271.6	37.12	358.85	112.8	-	-	-	-	372.01
⑧	Clay	5	16.2	-	143.2	293.9	42.70	412.80	143.2	-	-	-	-	427.95

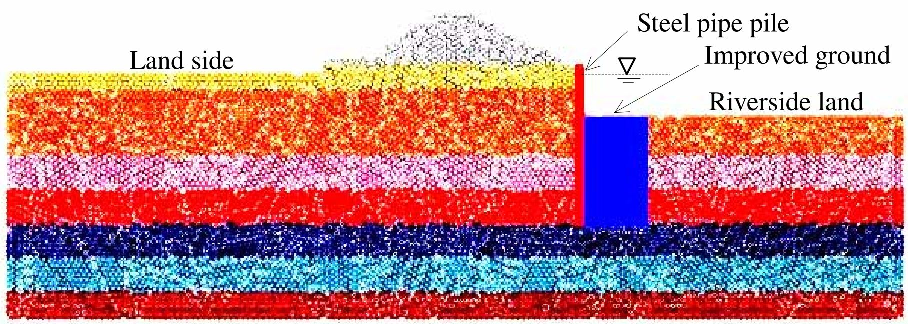

Figure 19 Improved ground model with steel pipe pile

pile (A value in parenthesis is the maximum vertical permanent displacement of embankment crest), in using the input wave in Yodo-gawa river dike shown in **Figure 13**. The deformation of the existing model without the prevention work in front of the revetment moves in the direction of both riverside land and land side due to liquefaction flow, and about 70% of the initial height (H) of embankment settles ($H\times$ 0.7). Although the horizontal displacement at the top of pile in case of the steel pipe pile model is about 2.0m, the vertical displacement of embankment crest ($H\times0.54$) is smaller that by the existing model. In case of the improved ground model with steel pipe pile, the horizontal displacement at the top of pile is about 0.7m, and the vertical displacement of embankment crest ($H\times0.47$) is less than 50% of the initial height of embankment. Also, the occupied liquefied zone areas in the shallow sandy layers is much smaller generally. However, the movement toward the land side is observed. In taking **Table 4** for practicing design into consideration, the safety factor (Fs(Δu)) obtained by the results of analysis is occupied within the limits of 0.6～0.8. As a result, Fs(Δu) would not be satisfied with the safety factor by practicing design maintaining more than 1.0 at least.

There is an implied requirement that the reasonable earthquake resistant method withstands the strong ground motion of the near-field earthquake. **Figure 21** shows the input wave (Maximum acceleration: approximately 717gal) of the strong ground motion which were observed at G.L.-83m in the Kobe Port Island vertical array on reclaimed land operated by Kobe city (Ejiri et al. [18]). **Figure 22** shows the comparison of acceleration response spectra with 5% damping which been obtained at Yodo-gawa river dike shown in **Figure 13** and the Kobe Port Island done in **Figure 21**. The acceleration response of the Kobe Port Island wave is stronger as twice or three times as that of Yodo-gawa river dike wave in the period from 0.1 to 5.0 second. **Figure 23** shows the deformation with excess pore water pressure ratio expressed by the degree of green color dots (0.2, 0.4, 0.6, 0.8) at 25 second obtained by the improved ground model with steel pipe pile in using the Kobe Port Island wave. Even though the horizontal displacement (about 0.9m) at the top of pile in this case is a few larger than that (about 0.7m) in **Figure 20(c)**, the vertical displacement (about 3.3m) of embankment crest in this case is nearly identical with that (about 3.3m) in **Figure 20(c)**. Despite the input wave with strong ground motions in the heavy earthquake, the drastic difference of deformation is not observed. Therefore, an input wave with strong ground motions in the heavy earthquake would exhibit the upper limit value for which the embankment would collapse.

There are plans to construct an improved ground at land side of a river dike in the near future and a need to estimate the seismic resistance in adopting that method. **Figure 24** shows the distinct elements by the improved ground model at land side. The parameters of improved

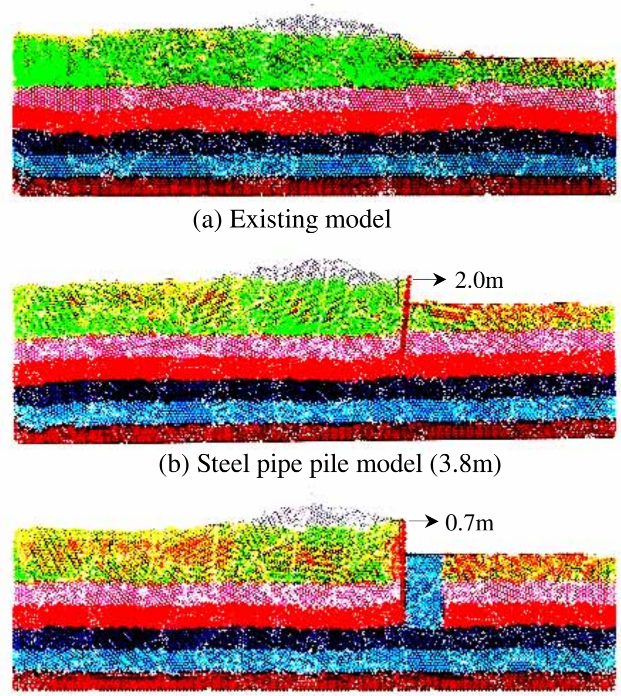

(a) Existing model

(b) Steel pipe pile model (3.8m)

(c) Improved ground model with steel pipe pile (3.3m)

Figure 20(a)(b)(c) Existing model, steel pipe pile model and improved ground model with steel pipe pile

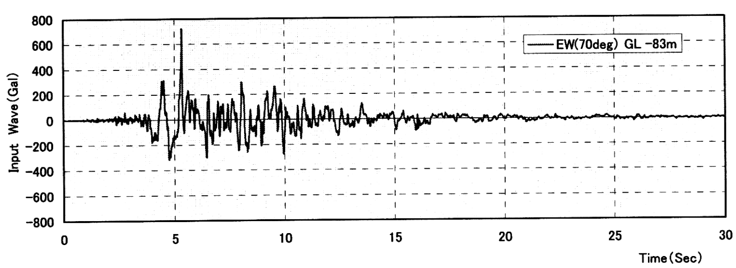

Figure 21 Input wave (The Kobe Port Island)

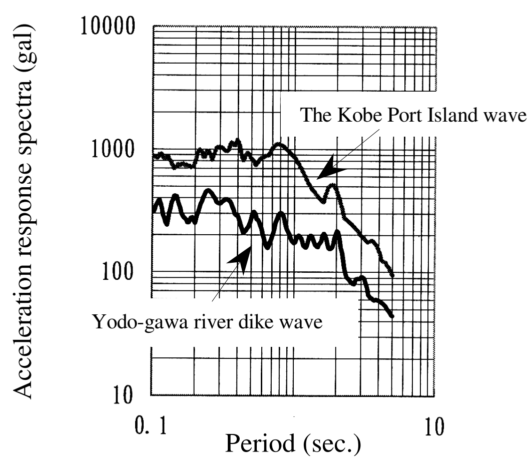

Figure 22 Acceleration response spectra

ground model at land side is assumed to be equal to the improved ground materials (No.4 and No.5) shown in **Table 7**. The deformation with excess pore water pressure ratio at 25 second obtained by the input wave of Yodo-gawa river dike shown in **Figure 13**, is shown in **Figure 25(a)**. And, the deformation with excess pore water pressure ratio at 25 second obtained by the input wave of the Kobe Port Island shown in **Figure 21**, is shown in **Figure 25(b)**. Despite the different input waves, the vertical displacements (about 2.5m) at the embankment crest in both cases are approximately same value, and that of the improved ground model at land side is smaller than that of the unimproved ground model at land side shown in **Figure 20(c)** and **Figure 23**. Especially, although the horizontal displacement (about 1.4m) at the top of pile in the improved ground model at land side shown in **Figure 25(b)** is larger than that (about 0.9m) at the top of pile shown in **Figure 23**, the bending moment at 25 second by analysis exhibits less than the allowable limits (SKY-400 and SKY-490). As a result of analysis, it is impossible to indicate the effectively of improved ground method at land side with steel pipe pile to prevent damage from liquefaction flow.

CONCLUSIONS

We have developed a calculating program for liquefaction flow by using DEM and introducing Iwan model, and the liquefaction analysis method is applied to Yodo-gawa river dike and Naka-gawa river.

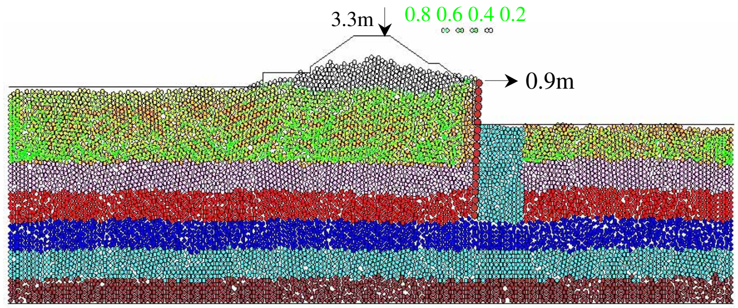

Figure 23 Deformation with excess pore water pressure ratio (The Kobe Port Island wave)

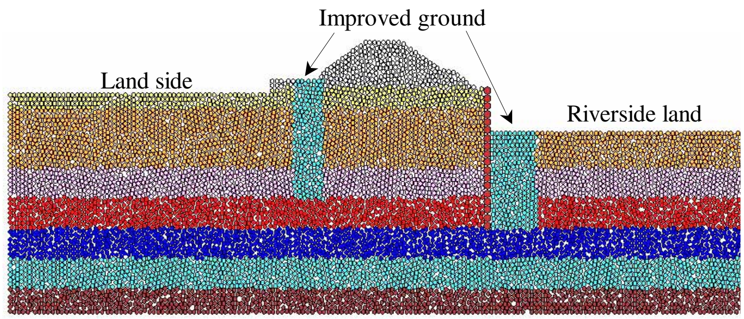

Figure 24 Distinct elements by improved ground model at land side

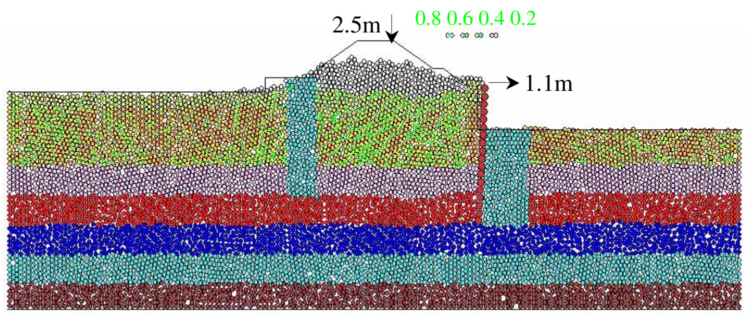

Figure 25(a) Deformation with excess pore water pressure ratio at land side (Yodo-gawa river dike wave)

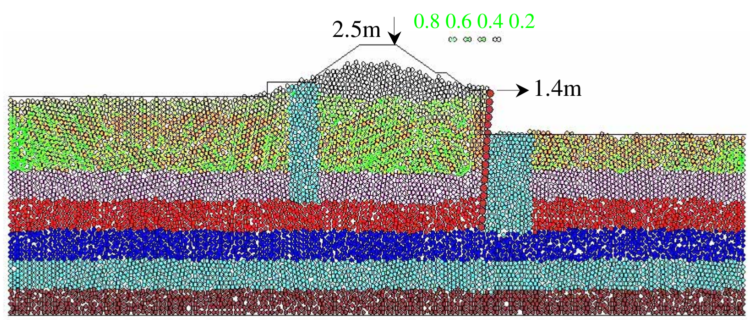

Figure 25(b) Deformation with excess pore water pressure ratio at land side (The Kobe Port Island wave)

Despite different disc radii (R=30, 15, 7.5cm) obtained by simple shear test, the results of analysis are approximately identical with the experimental results obtained by real specimen test. Particularly, in the case of R=7.5cm, the distribution of excess pore water pressure ratio for cyclic simple shear test obtained by analysis tends to coincide with σ_1 direction inclining to $\pi/4$ from horizontal.

The vertical displacement of embankment crest by damaged model in Yodo-gawa river dike, is larger than that by non-damaged model with a major bed. And, the former has good agreement with the actual measured maximum vertical permanent displacement. Although the vertical permanent displacement of embankment crest tends to decrease relatively in accordance with the decrease of disc radii, it seems improbable to change when performing the analysis using the distinct elements of R=30cm.

The vertical displacement of embankment crest in case of the improved ground model with steel pipe pile at riverside land in Naka-gawa river dike, is less than 50% of the initial height of embankment. And, the occupied liquefied zone areas in sandy layers is much smaller in comparison with both the existing model and steel pipe pile model. However, the movement in the direction of land side is observed. Also, the deformation of embankment crest obtained by the improved ground model at land side is smaller than that by the unimproved ground model at land side. Despite different input waves, the difference of deformation at embankment crest in employing the improved ground method, is not observed.

This analysis method can indicate the effectively of improved ground method or steel pipe pile to prevent damage from liquefaction flow, and provide satisfactorily enough estimation to correlate results of real disaster.

REFERENCES

1. Mori H, Ogawa Y, Kusano K, Okamoto J and Abe H. "Centrifuge Dynamic Modeling Test and Two-dimensional Liquefaction Analysis for Huge River Dike." 12WCEE, 2000: No.0476.
2. Abe H, Mori H, Fukutake K and Fujikawa S. "Investigation and Analytical Evaluation of Damage to Levee Caused by Liquefaction in Hyogoken-Nambu Earthquake." Proc. of JSCE, No.568/Ⅲ-39, 1997: 89-99 (in Japanese).
3. Matsuo O, Okamura M, Shimazu T and Nishi K. "Application of Finite Element Method to Liquefaction Problem." Public Works Research Institute Ministry of Construction, Vol.40, No.8, 1998: 50-55 (in Japanese).
4. Cundall PA and Strack ODL. "A Discrete Numerical Model for Granular Assemblies." Geotechnique, Vol.29, No.1, 1979: 47-65.
5. Ng TT and Dobry R. "Numerical Simulations of Monotonic and Cyclic Loading of Granular Soil." J. Geotech. Engrg., ASCE, Vol.120, No.2, 1994: 388-403.
6. Matsushima T and Kanagai K. "Grain-Shape effect on Peak Strength of Granular Materials." Computer Methods and Advances in Geomechanics, Desai et al.(eds), 2001: 361-366.
7. Ogawa Y, Mori H, Kusano K, Bercin AN, Gao G and Kameoka H. "Liquefaction Flow Analysis of River Dikes with Distinct Element Method." Proc. 35th Japan National Conference on Soil Mechanics and Foundation Engineering, 2000: 1637-1638 (in Japanese).
8. Mori H, Kusano K, Ogawa Y, Cao G and Kameoka H. "Liquefaction Analysis of River Dikes with Distinct Element Method." Proc. 36th Japan National Conference on Soil Mechanics and Foundation Engineering, 2001: 1373-1374 (in Japanese).
9. Iwan WD. "A Distributed-element Method for Hysteresis and its Steady-state Dynamic Response." Transactions of the ASME, Jour. App. Mech., Vol.33, No.4, 1966: 893-900.
10. Ogawa Y, Kusano K and Abe H. "Dissipative Energy and Stored Elastic Energy during Liquefaction Process." 12WCEE, 2000: No.1984.

11. Ogawa Y, Abe H and Yoshitsugu S. “Energy Loss and Stored Elastic Energy during Liquefaction process.” Earthquake Geotechnical Engineering, Ishihara (ed.), 1995: 957-962.
12. Ogawa Y. “One Dimensional Response Analysis during Earthquakes on Effective Stress Method.” Annual Report of Institute of Civil Engineering of Tokyo Metropolitan Government, 1989: 281-297 (in Japanese).
13. Meguro K and Hakuno M. “Fracture Analysis of Concrete Structure by Granular Assembly Simulation.” Bulletin of the Earthquake Research Institute, University of Tokyo, Vol.63, Part4, 1988: 409-468 (in Japanese).
14. Igarashi S and Meguro K. “Analysis of Per-anent Ground Deformation due to Liquefaction with Distinct Element Model.” Proc. of JSCE, No.424/Ⅲ-14, 1990: 271-282 (in Japanese).
15. Abe H and Kusano K. “Liquefaction Potential of Ground by the Non-linear Dynamic Analysis added Hysteretic Model in Finite Elements.” Annual Report of Institute of Civil Engineering of Tokyo Metropolitan Government, 1990: 293-306 (in Japanese).
16. Matsuo O, Okamura M, Uzuoka R and Mihara M. “Numerical Analyses of the Damaged Dikes in the 1995 Hyogoken-Nanbu Earthquake.” 12WCEE, 2000: No.0621.
17. Yoshihiro S. “Experimental Study on Lateral Resistance of a Pile with Embedded Head in sand.” Report of the Port and Harbor Research Institute, Vol.23, No.2, 1984: 75-179.
18. Ejiri J, Sawada S, Goto Y and Toki K. “Peak Ground Motion Characteristics.” Special Issue of Soils and Foundations, 1996: 7-13.